International Journal of Pharmaceutics 644 (2023) 123334

Contents lists available at ScienceDirect

International Journal of Pharmaceutics

journal homepage: www.elsevier.com/locate/ijpharm

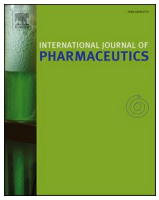

Non-invasive management of rheumatoid arthritis using hollow microneedles as a tool for transdermal delivery of teriflunomide loaded solid lipid nanoparticles

Heba Abd-El-Azim [a], Haidy Abbas [a,*], Nesrine S. El Sayed [b], Ahmed M. Fayez [c], Mariam Zewail [a]

[a] Department of Pharmaceutics, Faculty of Pharmacy ,Damanhour University, Damanhour, Egypt
[b] Department of Pharmacology and Toxicology, Faculty of Pharmacy, Cairo University, Cairo, Egypt
[c] Department of Pharmacology, School of Life and Medical Sciences, University of Hertfordshire Hosted by Global Academic Foundation, New Administrative Capital, Cairo, Egypt

ARTICLE INFO

Keywords:
Hollow microneedles
Disease modifying anti-rheumatics
Autoimmune diseases
Antigen induced arthritis
Trans-epidermal delivery

ABSTRACT

Conventional RA treatments required prolonged therapy courses that have been accompanied with numerous side effects impairing the patient's quality of life. Therefore, microneedles combined with nanotechnology emerged as a promising alternative non-invasive, effective and self-administrating treatment option. Hence, the main aim of this study is to reduce the side effects associated with systemic teriflunomide administration through its encapsulation in solid lipid nanoparticles (TER-SLNs) and their administration through transdermal route using AdminPen™ hollow microneedles array in the affected joint area directly. *In vitro* characterization studies were conducted including particle size, zeta potential, encapsulation efficiency and *in vitro* drug release. Also, *ex vivo* insertion properties of AdminPen™ hollow microneedles array was carried out. Besides, *in vivo* evaluation in rats with antigen induced arthritis model were also conducted by assessment of joint diameter, histopathological examination of the dissected joints and testing the levels of TNF-α, IL1B, IL7, MDA, MMP 3, and NRF2 at the end of the experiment. The selected TER-SLNs formulation was about 155.3 nm with negative surface charge and 96.45 % entrapment efficiency. TER-SLNs had a spherical shape and provided sustained release for nearly 96 h. *In vivo* results demonstrated that nanoencapsulation along with the use of hollow microneedles had a significant influence in improving TER anti-arthritic effects compared with TER suspension with no significant difference from the negative control group.

1. Introduction

Rheumatoid arthritis (RA) is a complicated inflammatory autoimmune disease that may be triggered by a variety of environmental and genetic factors. In joints RA causes invasive inflammation that may lead to joint disability. RA possesses several extra-articular implications as it may affect the gastrointestinal tract, the heart leading to ischemic heart diseases and it may also affect the pulmonary tissues (Wang et al., 2021; Zewail et al., 2021). RA conventional treatment approaches includes the administration of non-steroidal anti-inflammatory drugs and glucocorticoids for pain and inflammation control. Disease modifying antirheumatic drugs (DMARDs) are also used to suppress joint damage.

Generally, RA management requires long-term administration of oral therapies and injections (Gottenberg et al., 2019; Anita, 2021). Unfortunately, these conventional therapeutic strategies cause many side effects including gastrointestinal and extra-articular adverse reactions, short half-life, lack of selective drug localization and reduced patient compliance leading to poor patient commitment throughout the long-term treatment course and thereby, inconvenient therapeutic outcomes (Wang et al., 2022; Gorantla et al., 2022). Consequently, transdermal route surfaced as an alternative way for RA treatment securing a variety of benefits including bypassing the hepatic first-pass metabolism, avoiding off-target adverse effects, rapid onset of action (Gorantla et al., 2022). However, only a limited number of drug molecules can effectively penetrate the intact stratum corneum due to the perfect barrier function of the skin and the physicochemical properties of the penetrant molecule (Larraneta, 2016). Specifically, in RA treatment, the joint capsule represents an additional barrier to transdermal drug

* Corresponding author.
E-mail addresses: haidy.abass@pharm.dmu.edu.eg, haidy_miu2002@yahoo.com (H. Abbas).

https://doi.org/10.1016/j.ijpharm.2023.123334
Received 8 May 2023; Received in revised form 10 July 2023; Accepted 17 August 2023
Available online 19 August 2023

delivery (Shang et al., 2022). Interestingly, microneedling stands out as a simple and relatively low-cost approach for improving cutaneous drug penetration.

Microneedles (MNs) are an uprising skin delivery tool consists of micron-size pointed projections arranged in the form of an array (Zhang et al., 2022). Physically, MNs are designed to effectively penetrate the stratum corneum without reaching the nerves' endings to avoid pain stimulation (Zhang et al., 2022). In addition to the advantages of transdermal route applications, MNs provide suitability for sustained and controlled drug delivery, efficient intradermal and transdermal drug availability, ease of treatment termination, applicability of high localized drug orientation, allowance of dose reduction, painless self-administration and overcoming needles' phobia (Wang et al., 2022; Larraneta, 2016). Thus, MNs could potentially improve both of therapeutic outcomes and patient's compliance in the treatment of RA.

The first use of MNs for the transdermal delivery of RA medications was reported by Russell Frederick Ross in 2010 in a US patent (Ross, 2016). In the following years, several studies investigated the feasibility of MNs for the delivery of various drugs for the management of RA. Interestingly, research on the implementation of MNs in RA treatment is growing. Hollow MNs, specifically, showed a strong potential in RA therapy. Hollow MNs are designed with a central or eccentric pore in the needle tip. Those pores represent the direct microconduit for the drug to pass flow into the skin layers (Abd-El-Azim et al., 2022). Upon skin insertion, hollow MNs create microchannels in the dermal layers allowing for vertical drug diffusion and promoting local drug accumulation resulting in improved localized pharmacological efficacy (Wang et al., 2022). Hollow MNs offer several advantages, such as securing an accurate adjustable dose of the delivered medication, controlling the rate of drug delivery and absence of restrictions on the administered drug formulation (Zhang et al., 2022; Yang et al., 2019). Concerning RA, hollow MNs were reported to be a better solution for delivering high-molecular-weight biological DMARDs, such as denosumab (Bushra, 2020) and JAK inhibitor tofacitinib (Carcamo-Martinez, 2021) with high efficacy.

Teriflunomide (TER) (A771726) is the active metabolite of leflunomide which is an approved disease modifying anti-rheumatic. TER exerts its anti-rheumatic effects through the inhibition of the dihydroorotate dehydrogenase enzyme which controls *de novo* pyrimidine biosynthesis and regulates RA associated autoimmune reactions (Osiri, 2003; Zewail et al., 2022; Zewail, 2022). TER has the ability to suppress the production of tumor necrosis factor (TNF)-α, proinflammatory cytokines and prostaglandins (Kobayashi et al., 2004). Also, TER can inhibit osteoclastogenesis and control osteoclast function to prevent bone and joint deterioration (Kobayashi et al., 2004). TER systemic administration has been associated with numerous gastrointestinal symptoms like diarrhea and colitis besides its serious side effects on the lungs and the liver (El-Setouhy et al., 2015; Zewail, 2021).

Nanocarriers' application in RA management has several merits as they can increase the solubility of poorly soluble drugs hence their dissolution rate and bioavailability will be improved. Nanocarriers can also prolong the circulation half-life of drugs, control drug release rate and provided targeted drug delivery (Zheng et al., 2021; Zewail, 2019). Solid lipid nanoparticles (SLNs) are considered an excellent alternative for liposomal and polymeric drug delivery systems especially for the delivery of lipophilic drugs (Saedi et al., 2018; Ng et al., 2015). SLNs are biocompatible, biodegradable nanocarriers that can be prepared on large scale using high pressure homogenization technique (Ghasemiyeh and Mohammadi-Samani, 2018). RA management by using nanomaterials can enhance the bioavailability of therapeutic agents and selectively target damaged joint tissue.

Integration of nanoparticles with MNs would be expected to enhance stability, bioavailability and targetability of pharmaceuticals (Alimardani et al., 2021). For our knowledge, this is the first report investigated the transdermal delivery of TER-SLNs assisted by hollow MNs for RA management. Initially, TER was encapsulated into SLNs, and then delivered into the arthritic joint using Hollow MNs as a promising user-friendly and minimally invasive transdermal delivery approach for effective treatment of RA.

2. Materials

Teriflunomide was purchased from MedKoo Biosciences (North Carolina, USA). Compritol and pluronic (F127) were kind gifts from Gattefossé (Saint-Priest, France) and Pharco Pharmaceutical Companies (Alexandria, Egypt), respectively. Complete Freund's adjuvant (CFA) was obtained from Sigma-Aldrich (Steinem, Germany). AdminPen™ hollow microneedle arrays were purchased from NanoBioSciences LLC, USA.

3. Methodology

3.1. Preparation of TER-SLNs

TER loaded SLNs were prepared by melt emulsification method previously reported by Zewail et al. (Zewail, 2021) as follows, 100 mg of compritol was melted at 80 °C then 10 or 15 mg of TER was added to the melted lipid. Meanwhile an aqueous phase composed of 0.2 or 0.4 % F127 was heated to the same lipid phase temperature and added to the lipid/drug mixture while stirring on the magnetic stirrer. Then ultrasonication using probe sonicator at 60 mA for 5 min was carried out. Then, the resultant pre-emulsion was mixed with a secondary aqueous phase composed of deionized water and sonicated for extra 5 min an ice bath to obtain the final nanodispersion. The final dispersion was stored in the refrigerator was further investigation. Fig. 1A shows a schematic representation for the preparation of TER-SLNs by melt emulsification method.

3.2. Skin sampling preparation and intradermal injection using AdminPen™ hollow microneedles array

Intact full-thickness human skin was obtained from a male volunteer after abdominal plastic surgery. In brief, subcutaneous fats were removed using surgical scissors. Skin surface was rinsed by normal saline solution, left to dry, wrapped in aluminum foil and kept at −20 ∘C until further use as these were reported to be the optimum conditions for storing human skin for 3–6 months (Dragicevic-Curic et al., 2010).

Both TER solution and TER-SLNs were injected into the upper surface of the cleaned full-thickness human skin using AdminPen™, 43 stainless steel metallic Ho-MNs of 1200 μm length located within 1 cm^2 of circular MN array, Fig. 1B. Before application to skin, AdminPen™ was connected to a syringe prefilled with TER-SLNs. The thumb and the index finger were used to insert the AdminPen™ Ho-MNs into the skin.

3.3. In vitro characterization of TER-SLNs

3.3.1. Particle size and zeta potential measurement

Particle size, polydispersity index (PDI), and zeta potential values were assessed using a Zeta sizer Nano ZS (Malvern Instrument, UK) at a scattering angle of 173° at 25 °C.

3.3.2. Entrapment efficiency (EE%)

EE % was indirectly evaluated utilizing Centrisart®-I tube (MWCO 300 kDa, Sartorius AG, Gottingen, Germany). TER-SLNs were centrifugated for 30 min at 5000 rpm to separate free unencapsulated TER. After that, the concentration of free unencapsulated TER was determined using HPLC equipped with UV detector at 305 nm (Zewail, 2022).

$$EE(\%) = \frac{Total\ TER\ concentration - concentration\ of\ unencapsulated\ TER}{Total\ TER\ concentration} \text{x}100$$

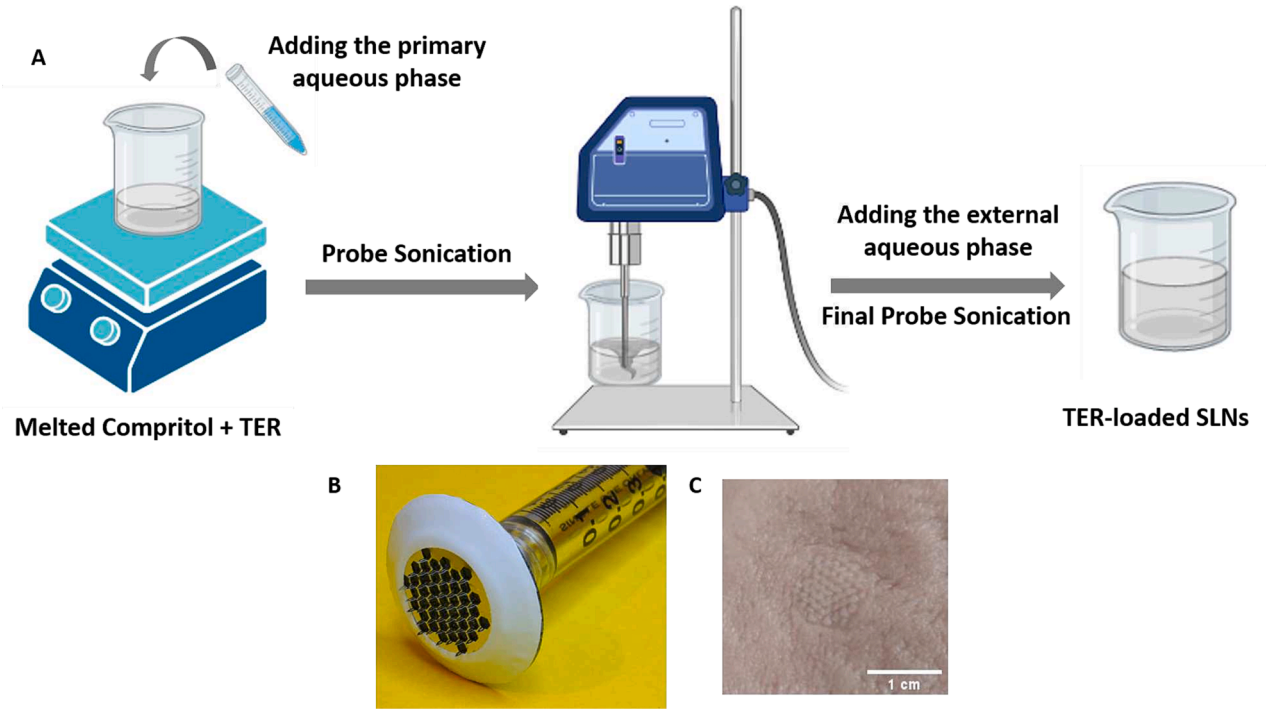

Fig. 1. A) A schematic representation for the preparation of TER-SLNs by melt emulsification method. B) AdminPen™ hollow MNs showing 43 stainless-steel MN shafts of 1200 μm in length and 1 cm^2 in area (Image was used with permission from AdminMed). C) Image photographed by a standard mobile camera (Samsung Galaxy Note8, 12 MP, dual pixel, PDAF) illustrating excised full-thickness human skin after insertion of AdminPen™ 1200 μM Ho-MN array.

3.3.3. Drug loading (DL %)

TER loaded SLNs formulations were freeze dried and drug loading (DL) was estimated by measuring TER concentration in a given weight of freeze-dried NLCs.

$$DL(\%) = \frac{concentration\ \ of\ \ encapsulated\ \ TER}{weight\ \ of\ \ NLCs} \text{ x } 100$$

3.3.4. Morphological evaluation

The morphology of selected TER-SLNs formulation was examined using transmission electron microscope (TEM; JEM-100CX; JEOL, Japan) after staining with uranyl acetate.

3.3.5. In vitro drug release and release kinetics

In vitro release studies of different TER-SLNs formulations were carried out by dialysis technique. Different TER-SLNs formulations were put in dialysis bags that contain 0.5 mg of TER and immersed in 75 ml of PBS (pH 7.4) to ensure that sink conditions are attained. Bags were incubated in a shaking water bath at 37 ± 0.2 °C and 100 rpm. At prearranged time intervals, samples were withdrawn and replaced with fresh PBS. The amount of TER released was determined by HPLC method at 305 nm (Zewail, 2022). The experiment was carried out in triplicates.

Release data were fitted to zero order, first order, Higuchi, Krosmeyer Peppas models and R^2 values were determined using DD solver software.

3.3.6. Stability study

Particle size, entrapment efficiency, PDI were revaluated for the selected TER SLNs formulation after 3 months of storage at 4 °C.

3.4. Ex vivo insertion properties of AdminPen™ hollow microneedles array

The skin penetration capabilities of AdminPen™ hollow MNs were assessed as previously described with some modifications (Abd-El-Azim et al., 2022). The MNs were inserted into full-thickness human skin, as stated in Section 3.2. Following the removal of MNs, digital images were captured for the skin using Samsung Galaxy Note8, 12 MP, dual pixel, PDAF. The number of visible holes created by hollow MNs was counted and the percentage of percutaneous penetration was also determined according to the following equation:

$$The\ \ percentage\ \ of\ \ penetration = \frac{Number\ \ of\ \ created\ \ holes\ \ in\ \ skin}{Total\ \ number\ \ of\ \ hollow\ \ microneedles} \times 100$$

3.5. In vivo evaluation of TER-SLNs

3.5.1. Experimental animals

Thirty-two adult male wistar rats with an average weight of 150–170 g were divided into four groups (n = 8) The rats had free access to water and diet and were kept for one week before the experiment to adapt. Both temperature and humidity were controlled at 22 ∘C ± 1 and 60 ± 10%, respectively. Animal handling during the experiments was carried according to the guidelines for the Care and Use of Laboratory Animals (NIH Publication, 2011, 8th Edition) followed by the Faculty of Pharmacy, Cairo University, with the permit number PT 3189.

3.5.2. Induction of rheumatoid arthritis

Rats were anesthetized with an intraperitoneal injection of ketamine (50 mg/kg) and xylazine (10 mg/kg), afterwards, RA induction was carried out on all groups with exception of the negative control. RA

induction was conducted using antigen induced arthritis model (AIA) as previously reported (Zewail et al., 2021; Zewail, 2022; Zewail, 2019; Abbas et al., 2021). In brief, 0.2 ml of complete Freund's adjuvant (CFA) was intra-articularly injected in the right knee of each rat, whereas the left knee was kept as control.

3.5.3 Experimental design

Animals (n = 8/group) were divided randomly into four groups as Fig. 2. RA induction was carried out on all groups with exception of the negative control. Group 1: (Positive control) Rats were injected by 0.2 ml of complete Freund's adjuvant (CFA) through intra-articular injection at the first day of the experiment, at days 3 and 10 rats will receive 0.1 ml saline by intradermal injection. Group 2: Rats were injected by 0.2 ml of CFA through intra-articular injection at the first day of the experiment then received 2 intradermal injections (using AdminPen™ hollow microneedles in the joint area) of teriflunomide suspension10 mg/kg (Zewail, 2022) at day 3 and 10 of the experiment. Group 3: Rats will be injected by 0.2 ml of CFA through intra-articular injection at the first day of the experiment then received intradermal injection of teriflunomide loaded nanocarriers (TER-SLNs,10 mg/kg) (Zewail, 2019) at day 3 and 10 of the experiment. Teriflunomide dose will be. Group 4: (Negative control) Rats received normal saline through the intradermal route.

After 14 days, rats were anesthetized and sacrificed by cervical dislocation under anesthesia with ketamine (50 mg/kg) and xylazine (10 mg/kg) (Boskabady, 2011) and Joints of 3 animals were fixed in 10% (v/v) formalin for 24 h to perform histopathological examination. For other animals, serum samples were collected and centrifuged at 5000 rpm at RT for 15 min then the serum was frozen at − 80 °C until further analysis. All efforts were made to minimize animal suffering and to reduce the number of animals used.

Average rat knee joint diameters were evaluated at days 0, 3, 7 and 14 of the experiment by a micrometer (KM-211–101, Shaanxi, China).

3.5.4. Enzyme linked immunosorbent assay (ELISA)

At the end of the experiment, serum levels of tumor necrosis factor-alpha (TNF-α), interleukin 1B (IL1B), interleukin 7 (IL7) (My BioSource, San Deigo, CA, USA), malondialdehyde (MDA), matrix metalloproteinases 3 (MMP 3), and nuclear factor (erythroid-derived) Like 2 (NRF2) (Cusabio Technology LL, Houston, USA), were estimated utilizing ELISA kits according to the manufacturer instructions.

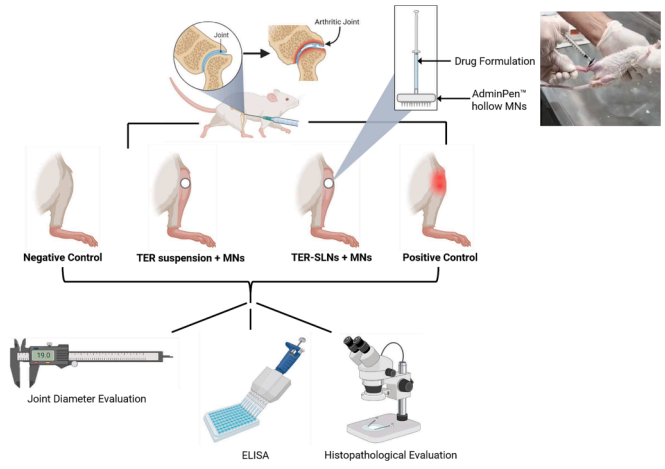

Fig. 2. Schematic representation showing the different treatment groups investigated in the in vivo study and further characterization techniques. Intradermal administration of drug formulations using AdminPen™ hollow MNs into the inflamed rheumatic joint in rats.

3.5.5. Histopathological evaluation

Histopathology specimen were kept in 10 % neutral buffer formalin, then histologically processed through formic acid decalcification, trimming, washing with water, dehydration in ascending grade of ethyl alcohol followed by their clearing in xylene and embedding in paraffin. Thin sections (4–6 μ) were processed and stained with hematoxylin and eosin stain and Masson's Trichrome stain.

3.6. Statistical analysis

All the results are presented as mean ± SD. Statistical analysis of colloidal characteristics of SLNs, joint diameter measurements and ELISA were conducted by Student's t-test ($P < 0.05$), Two-way ANOVA followed by Tukey's test ($P < 0.0001$) and One-way ANOVA followed by Tukey's test ($P < 0.0001$), respectively using Prism 7 software.

4. Results and discussion

4.1. In vitro characterization of TER-SLNs

4.1.1. Colloidal properties

TER and its parent drug leflunomide are hydrophobic drugs belonging to biopharmaceutical class II (Zewail et al., 2022; Zewail, 2019; El-Sayyad et al., 2017). SLNs were chosen for preparing TER nanocarriers based on its several merits as they are biocompatible, easy to scale up, has high drug loading capacity and can provide sustained drug release pattern (Zewail, 2021; Ghasemiyeh and Mohammadi-Samani, 2018). Hot homogenization technique was chosen for TER-SLNs preparation as this method avoids the use of organic solvents and hence can reduce toxicity hazards (Zewail, 2021; Venkatesh, 2011). Also, this method is more suitable for lipophilic drugs compared the cold homogenization method which is employed for hydrophilic drugs (Üner and Yener, 2007). TER-SLNs were prepared using (0.2 and 0.4 % w/v) F 127 and (10 and 15 mg) of TER as illustrated in Table 1. As Fig. 3A shows, increasing F 127 concentration from 0.2 % to 0.4 % resulted in a significant reduction in particle size (student t-test $p < 0.05$). Particle size of SLN 1 and SLN 3 both contain15 mg of TER and composed of 0.2 and 0.4 % F127 was significantly reduced from 305.5 to 198.8 nm, respectively. Also, particle size of SLN 2 and SLN 4 was reduced from 237.6 to 155.3, respectively upon doubling F 127 concentration.

F127 is composed of non-linear hydrophobic chains that can arrange themselves within the lipid layer, this will strongly influence particle compaction and can eventually lead to particle size reduction (Mistry and Sarker, 2016). Higher F 127 concentrations can reduce particle's surface tension and lead to particle size reduction (Zirak and Pezeshki, 2015). Our findings are in agreement with previously reported results (Zewail, 2019; Zirak and Pezeshki, 2015).

The effect of TER concentration was also studied (Table 1). Increasing TER concentration from 10 to 15 mg resulted in a significant increase in particle size. For example, particle size of SLN 2 (composed of 10 mg TER) and SLNs (composed of 15 mg TER) were 237.6 and 305.5 nm, respectively.

PDI is considered an indication of nanodispersion homogeneity. PDI values<0.3 is considered optimum, while values less 0.5 are within acceptable limits (Onugwu, 2022). The PDI values of the prepared TER-SLNs are considered within the acceptable limits suggesting formulations' homogeneity, the PDI values ranged from 0.225 to 0.397 (Table 1).

Zeta potential is an pivotal factor in nanocarriers' stability, formulations with zeta potential values around ± 30 mV are considered stable (Ahmed et al., 2020). This may be attributed to the repulsive forces that prevent particles coalescence and aggregation (Zewail, 2019; Ahmed et al., 2020; Rahman, 2013). All formulations carried negative surface charge as Table 1 illustrates. This is in agreement with previous results reported by Zewail et al. of the negatively charged TER loaded nanostructured lipid carriers (Zewail, 2022). Zeta potential values ranged

Table 1
Composition and colloidal characteristics of TER SLNs.

Formulation	Compritol Concentration	TER concentration	F 127 (% w/v)	Particle size (nm)	PDI	Zeta potential (meV)	DL %	EE %
SLN 1	100 mg	15 mg	0.2	305.5 ± 1.3	0.225 ± 0.9	− 22 ± 1.2	9.24 ± 0.8	97.12 ± 1.2
SLN 2		10 mg		237.6 ± 1.2	0.397 ± 0.8	− 20.7 ± 0.9	6.51 ± 0.4	96.67 ± 1
SLN 3		15 mg	0.4	198.8 ± 1	0.366 ± 0.6	− 21.2 ± 0.2	9.72 ± 0.5	97.34 ± 0.7
SLN 4		10 mg		155.3 ± 0.6	0.328 ± 0.2	− 19.4 ± 1	6.42 ± 0.2	96.45 ± 1.5

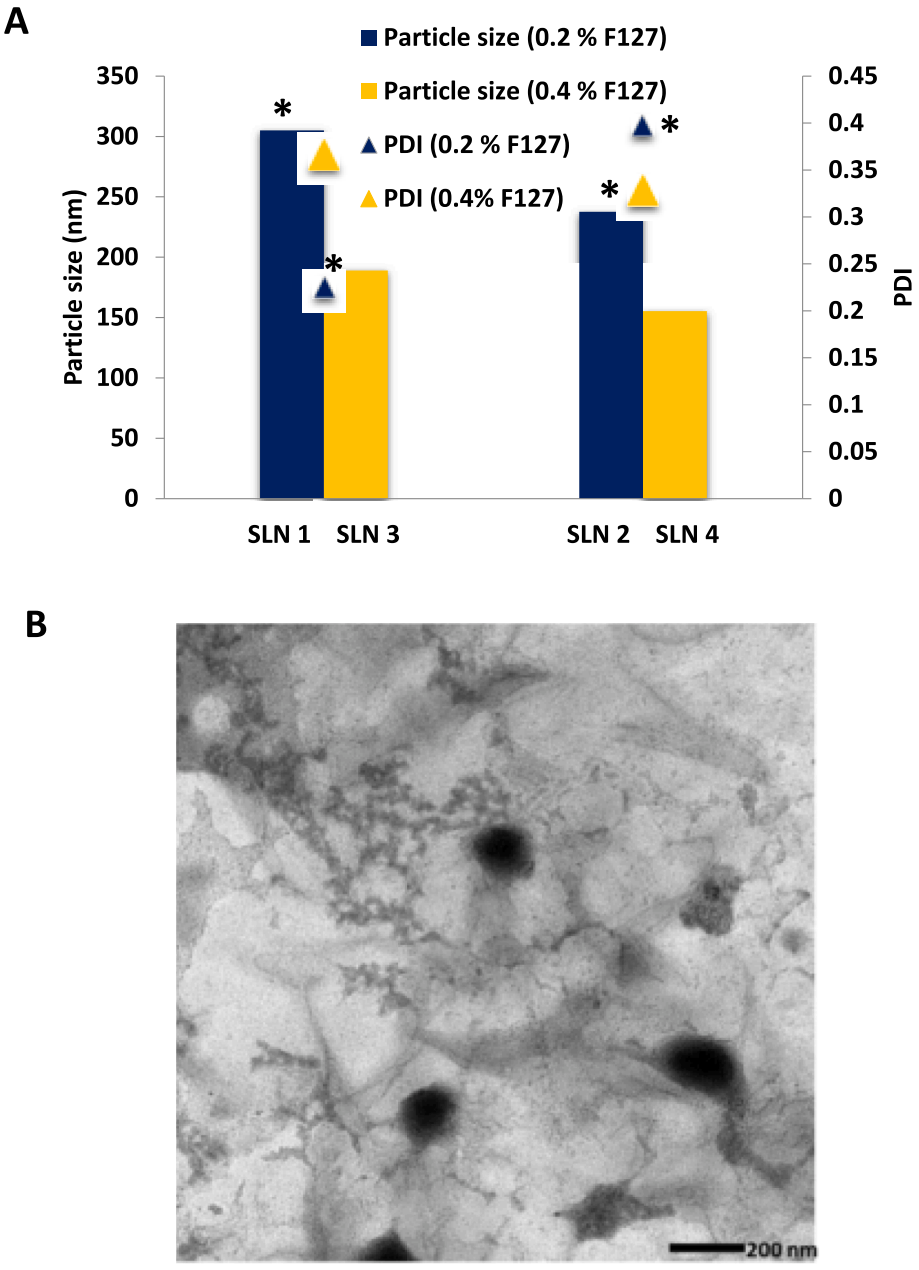

Fig. 3. (A) Effect of F127 concentration on particle size and PDI of TER SLNs, (B)TEM micrograph for selected formulation SLN 4. Statistical analysis of particle size and PDI were carried out using Student's *t*-test ($p < 0.05$), * statistically significant difference.

from – 19.4 (SLN 4) to –22 (SLN1). TER SLNs loaded with 15 mg TER (SLN 1, SLN 3) had a slightly higher negative zeta potential value compared to those loaded with 10 mg TER (SLN 2, SLN 4). This may be attributed to the negative surface charge of the drug (Zewail, 2019).

All TER-SLNs possessed high EE values that ranged from 96.45 to 97.34 %. The amount of drug that can be loaded in the delivery system is dependent on the physicochemical properties of drug and the preparation process. High EE % may occur as a result of high drug solubility in the melted lipid (Lastow et al., 2015). Also, compritol is composed of combination of mono-, di- and triacylglycerols that can accommodate more drug molecules in the spaces created between the carbon chains resulting in high EE % (Onugwu, 2022).

As Table 1 illustrates DL % increased by increasing TER concentration from 10 to 15 mg. DL % of SLN 1 (composed of 15 mg TER) and SLN 2 (composed of 10 mg TER) were 9.24 and 6.51, respectively. These findings are in agreement with the results previously reported by Zewail (2022).

4.1.2. *In vitro drug release and release kinetics*

In vitro drug release study was conducted for TER suspension and TER-SLNs in PBS pH 7.4 as Fig. 4 illustrates. All the formulations demonstrated biphasic release pattern that extended for 96 h. TER suspension was completely released within 48 h. Initial burst effect was noted in all the formulations. Amount of TER released after 30 mins was 12, 14, 13 and 15 % for SLN 1, SLN 2, SLN 3 and SLN 4, respectively (Fig. 4 insert). Burst effect may be attributed the adsorption TER on the surface of SLNs. Prolonged TER release may be assigned to the extended time needed for TER to diffuse from lipid matrix of SLNs to release medium (Abbas et al., 2018).

Percentage cumulative TER released was higher in TER suspension compared to all TER-SLNs formulations and this may be attributed to the ability of SLNs to provide extended TER release pattern. TER release rate was the highest in SLN 4 followed by SLN 3, SLN 2 and SLN 1. This may be attributed to the effect of particle size on the rate of drug release. The smaller the particle size the larger the surface area exposed to the release medium and hence release rate is increased compared with nanocarriers with larger particle size (El-Nabarawi et al., 2020; Abbas et al., 2021). This is in agreement with the results previously reported by Lastow et al. (Lastow et al., 2015) who reported the direct relation between SLNs particle size and release rate of budesonide from SLNs (Lastow et al., 2015).

Based on the aforementioned resulted, SLN 4 was selected for further characterization as it had suitable particle size (155.3 nm), PDI (0.328) and high entrapment efficiency (96.45 %).

Release data were fitted to zero order, first order, Higuchi, Krosmeyer Peppas models and R^2 values were recorded in Table 2. Krosmeyer Peppas model had the highest R^2 values in SLNs formulation while first order release model had the highest R^2 value for TER suspension. n values was<0.45 so SLNs formulations showed Fickian diffusion and the drug release mechanism is mainly through drug diffusion process (Onugwu, 2022).

Table 2
Release kinetics of different TER SLNs and TER suspension.

Release model	R^2				
	SLN 1	SLN 2	SLN 3	SLN 4	TER suspension
Zero order	0.789	0.771	0.684	0.695	0.530
First order	0.864	0.863	0.781	0.842	**0.951**
Higuchi	0.866	0.851	0.748	0.759	0.595
Krosmeyer and Peppas	**0.987**	**0.993**	**0.99**	**0.99**	0.931

4.1.3. *TEM examination*

As Fig. 3B illustrates that selected TER-SLNs formulation (SLN 4) had a spherical shape with a smooth morphology and no drug crystals suggesting the good encapsulation of TER within the SLNs.

4.2. *Intradermal injection of TER-SLNs using AdminPen™ hollow microneedles array*

Due to both skin and joint barriers, it is challenging to effectively deliver medications to the joint cavity using traditional transdermal applications (Shang et al., 2022). Therefore, throughout the last decade, MNs emerged as an advanced option for the management of RA. In this study, AdminPen™ hollow MNs were used to transdermally deliver TER-SLNs to the inflammatory sites.

The AdminPen™ hollow MNs are minimally invasive MN arrays designed to enable transdermal or intradermal delivery of liquid formulations according to the US Patent No. 7,658,728 (Yuzhakov and Microneedle array, patch, 2010). Each array is composed of 43 sharp-edged MN shafts of 1200 μm in length and 1 cm^2 in area. Each MN in the array is designed with off-centered hollow pore on its side. This innovative structure enabled for efficient drug delivery without needle blockage. Furthermore, the MNs are fabricated from the strong stainless-steel metal to avoid the occurrence of invisible damage due to needle breaking in skin. Upon skin application, the AdminPen™ device create

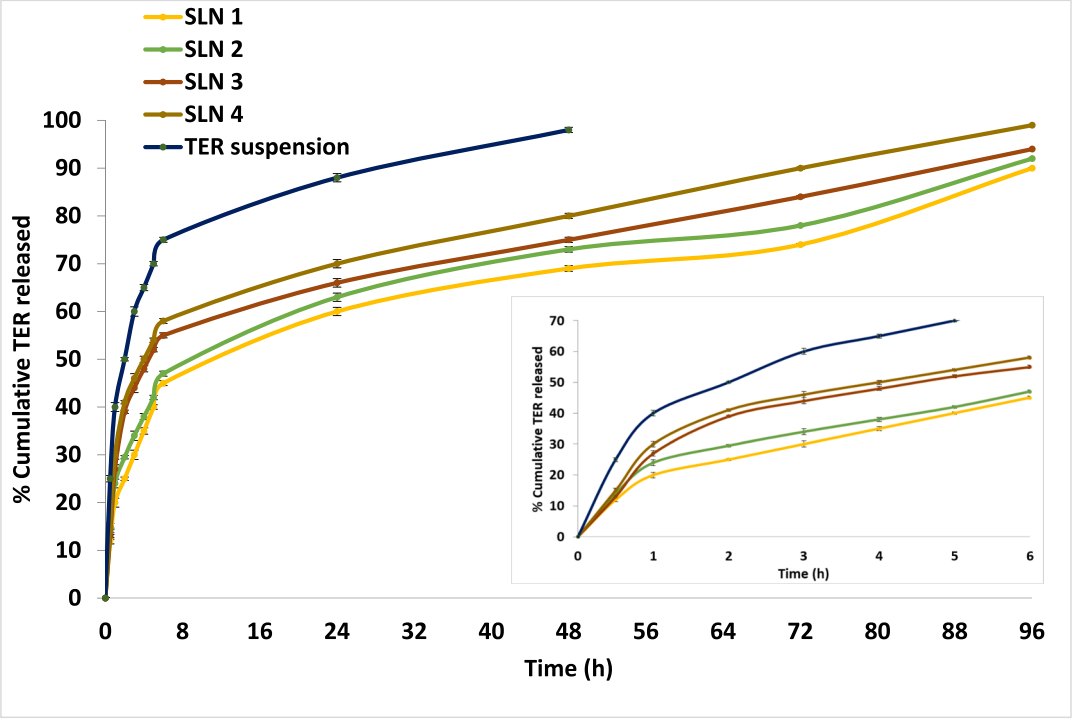

Fig. 4. Cumulative percentage TER released from different TER SLNs formulations.

tiny micropores in the stratum corneum and epidermis of about 1100 to 1200 μm in depth (Abd-El-Azim et al., 2022; Yuzhakov, 2010). The formed microchannels simply collapse and the skin barrier is quickly restored shortly after removal of the MNs from skin eliminating any possible risk for skin infection (Abd-El-Azim et al., 2022). Due to these interesting privileges, AdminPen™ hollow MNs were selected to deliver the prepared TER-SLNs deeply across the skin.

4.2.1. *Ex vivo insertion properties of AdminPen™ hollow microneedles array*

The action of MNs depends on its effective insertion, as the stratum corneum must be penetrated for the MN array to have its effect (Larrañeta et al., 2014). In other words, successful skin penetration via AdminPen™ hollow MNs is crucial for successful transdermal delivery of TER-SLNs. The penetration capabilities of MNs could be assessed through excised skin samples or through Parafilm M® as a skin model (Abd-El-Azim et al., 2022; Larrañeta et al., 2014). In a previous work, the author, Abd-El-Azim (Abd-El-Azim et al., 2022), proved the efficient insertion of the currently-used AdminPen™ hollow MNs through Parafilm M® membrane recording a penetration depth of 889 μm corresponding to more than 80% of the actual needles height. Excised human skin was reported to be the "gold standard" in *in vitro* testing (Abd, 2016). In the present study, the insertion properties of the AdminPen™ hollow MNs were evaluated in excised human skin. The generated images, Fig. 1C, showed complete insertion resulting in 43 dermal micropores representing the 43 MNs in the array with distinct interspacing distances. Thus, the observed efficient skin penetration reflected the strong mechanical strength of the applied MNs. Consequently, the proposed MN-SLNs combined delivery system revealed a promising potential for the deep transdermal delivery of TER to arthritic joints.

4.3. *In vivo study*

4.3.1. *RA induction*

RA was successfully induced in mice and rats by several models including AIA that had proven to be effective to produce RA associated physiological alteration (Choudhary et al., 2018). Liu et al. (Liu, 2009); Zewail et al. (Zewail, 2019); Kamel et al. (Kamel et al., 2016) and Abbas et al. (Abbas et al., 2021) among others have reported effective AIA induction using CFA in rats. AIA is characterized by rapid onset and progression of RA symptoms with distinctive joint swelling, cartilage degeneration and joint deformity (Zewail, 2021; Choudhary et al., 2018).

4.3.2. *Joint morphology and diameter measurements*

Morphological examination of joints at the end of the experiment (Fig. 5B) showed that the group treated with TER-SLNs using MNs had almost normal joint morphology and showed greater improvement compared with the group treated with TER suspension using MNs and the positive control group.

Average joint diameters of different experimental groups were estimated at days 0, 3, 7 and 14 of the experiment (Fig. 5A). Statistical data analysis using two-way ANOVA followed by Tukey test ($p < 0.0001$) revealed that treatment groups showed statistically significant differences from the positive control group. Importantly, the group treated with TER-SLNs using MNs demonstrated no statistically significant differences from the negative control.

4.3.3. *Elisa*

Different types of inflammatory markers contribute to the pathogenesis of RA such as IL-1 β and TNF α which act as the main players as they can control cell communication and regulate the expression of

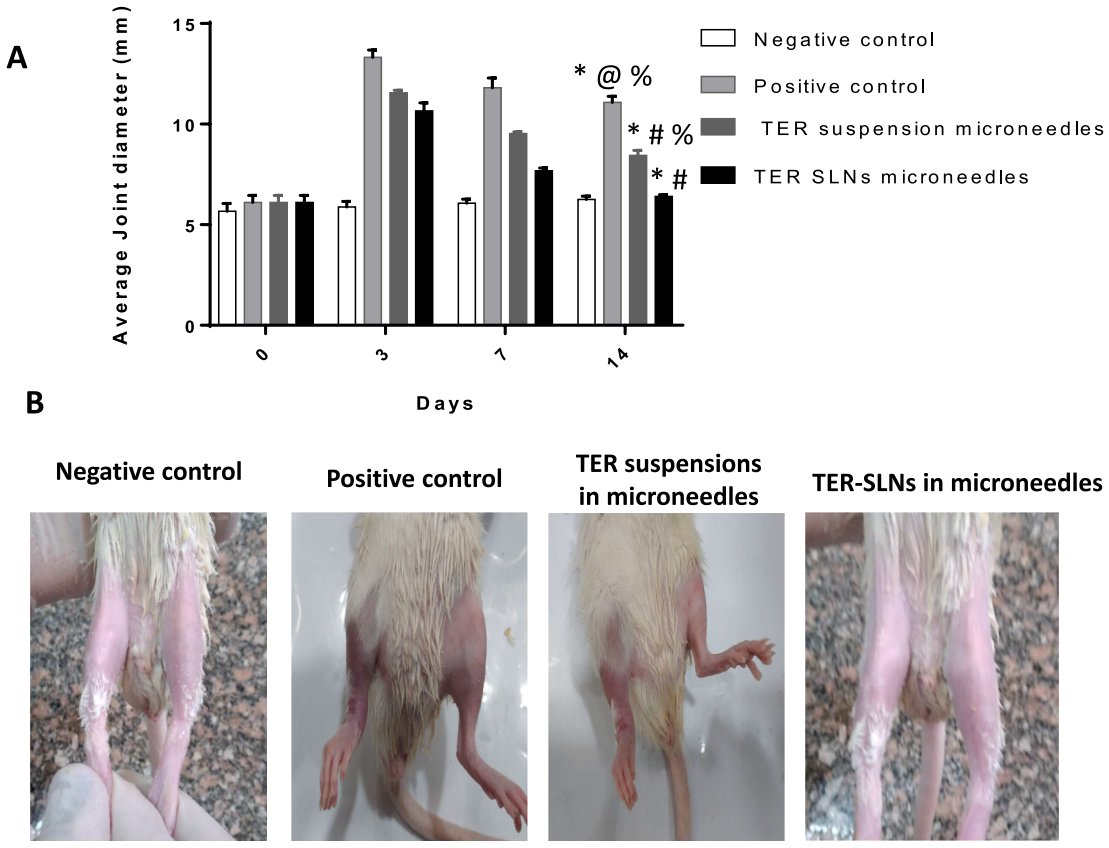

Fig. 5. (A) Average joint diameter of different experimental groups at days 0, 3, 7, and 14. (B) Joint morphology at the end of experiment. Statistical analysis using Two way ANOVA of joint diameter at the end of the experiment ($p < 0.0001$). * Significant difference from the negative control, # significant difference from the positive control, @ significant difference from TER suspension in microneedles and % significant difference from TER-SLNs in microneedles.

other inflammatory mediators. These mediators can stimulate chondrocytes and synovial cells to release MMPs that cause cartilage destruction. Previous reports suggested that IL-1 plays a more crucial role in the processes involved in joint destruction, while TNF has a more prominent role in progression of inflammation (Kutukculer et al., 1998).

Typically, IL-1β and TNF α increase the stromal production of IL-7 that in turns up-regulates the production of TNF α by macrophages. Also, IL-7 can stimulate the production of osteoclastogenic cytokines resulting in bone destruction (Churchman and Ponchel, 2008).

Beside IL 1, TNF α and IL 7, MMP-3 plays an important role in RA pathogenesis as it is produced in inflamed joints and released to the blood stream. Measurement of serum MMP-3 provides information about progression of rheumatoid diseases, and potentially response to treatment (Fadda et al., 2016; Sun et al., 2014).

Also, NRF2 has a crucial role in the regulation of many antioxidants, anti-inflammatory, cell survival genes as well as the regulation of immune responses. It can exert cellular defensive mechanisms to remove the cytotoxic electrophiles, reactive oxygen species and protect the tissues (Chadha et al., 2020; Ferrándiz et al., 2018).

RA is associated with increased production of reactive oxygen species. Cell membrane and its components such as proteins and lipids are oxidized and damaged by these free radicals. MDA is a byproduct of lipid peroxidation that can affect DNA and lead to cell death (Vyas et al., 2016; Chaturvedi, 1999). Increased levels of MDA and MDA-modified proteins were noted in RA patients and can reflect disturbances in oxidation balance occurring during systemic inflammation (Grönwall et al., 2017).

Serum levels of IL-1β, TNF α, IL 7, NRF2, MMP3 and MDA were estimated at the end of the experiment (Fig. 6). Levels of the aforementioned inflammatory biomarkers with exception of NRF2 level were

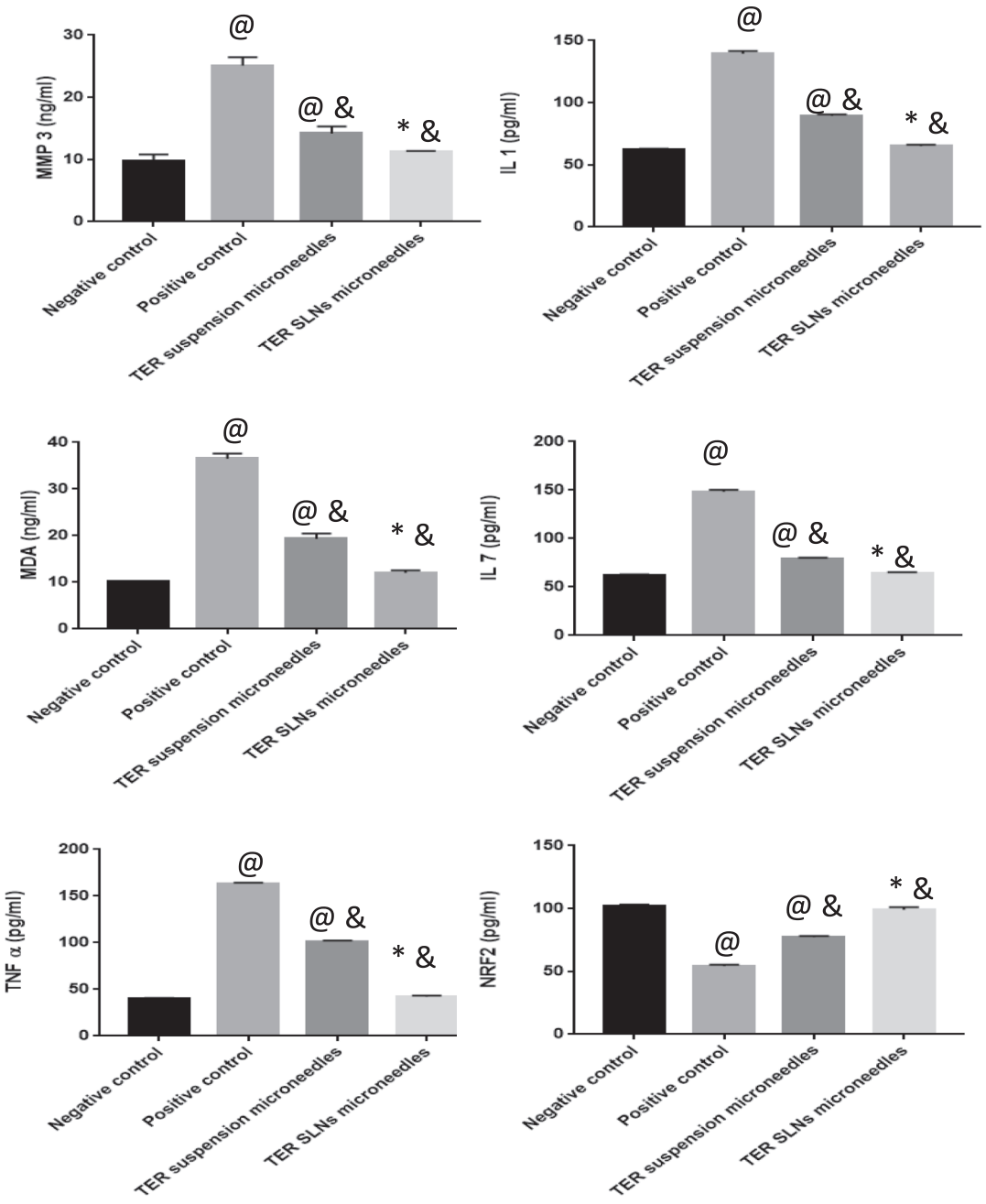

Fig. 6. Serum levels of different inflammatory biomarkers at the end of the experiments. Data analysis was conducted using one-way ANOVA followed by Tukey's test ($p < 0.0001$). @ significant from the negative control group. & significant from the negative control group. * significant from TER suspensions in microneedles.

elevated in the positive control group indicating successful RA induction. These findings were a long with previous reports of elevated serum levels of these markers in RA patients (Odobasic et al., 2014; Kamel et al., 2016; Fernandes et al., 2012; Abbas et al., 2022). As Fig. 6 illustrates, levels of IL-1β, TNF α, IL 7, MMP3 and MDA were lower in the treatment groups compared with the positive control group. On the other hand, NRF2 level was higher in treatment groups compared with the positive control group. For example, TNF α serum levels were 163.2, 101.2, 42, and 39.7 pg/ml for the positive control, group treated with TER suspension using MNs, group treated with TER-SLNs using MNs and the negative control group, respectively. Also, levels of MMP3 were 25.1, 14.2, 11.3 and 9.8 ng/ml for the aforementioned groups in the same order.

Levels of MDA increased by 3.5, 1.8, 1.1 folds in the positive control, the group treated with TER suspension using MNs and the group treated with TER-SLNs using MNs, respectively compared with the negative control group.

On the other hand, NRF2 level decreased by 1.88 and 1.32 folds in the positive control group and the group treated with TER suspension using MNs compared with the negative group. Meanwhile the group treated with TER-SLNs using MNs demonstrated nearly the same level as the negative control.

Statistical analysis of serum level data followed by Tukey test ($p < 0.0001$) showed that treatment groups showed statistically significant biomarkers levels compared with the positive control group. Treatment groups demonstrated significant differences among each other. On the other hand, no statistically significant differences were observed between the biomarkers' levels of the group treated with TER-SLNs using MNs and the negative control group.

4.3.4. Histopathological examination

Fig. 7A and B represent the photomicrograph of joints dissected from different experimental groups after histological processing and staining with Hematoxylin and Eosin and Masson Trichrome stains. The negative control group demonstrated normal histological structure of articular surface while roughness of articular surface with infiltration by mononuclear inflammatory cells (black arrow) and substitution with fibrous connective tissue (star) were observed in the positive control group. The group treated with TER suspension using MNs showed roughness and severe destruction of articular surface (red arrow) in addition to infiltration of mononuclear inflammatory cells. Interestingly, the group treated TER-SLNs using MNs demonstrated normal histological structure of articular surface in both Hematoxylin and Eosin and Masson-Trichrome stains.

Histopathological findings are along with the joint diameter and ELISA results. Superiority of TER suspension over the positive control group may be attributed to the ability of TER to inhibit dihydro-orotate dehydrogenase activity in addition to its ability to inhibit the production of T cells and the proinflammatory cytokines. TER can also inhibit TNF-α-induced NF-κB activation in numerous cell lines (Kirsch, 2005). Furthermore, TER can control osteoclast function which results in the alleviation of joint inflammation and prevention of joint destruction (Kobayashi et al., 2004; I Keen et al., 2013; Kirsch, 2005; Sanders and Harisdangkul, 2002). The superiority of TER-SLNs may be attributed to the effect of nanoencapsulation on increasing drug solubility and hence improving its pharmacological effects (Zewail, 2019). Importantly, the group treated with TER-SLNs using hollow MNs showed no statistically significant differences from the negative group in joint diameter, biomarkers levels and even in histopathological examination this may be attributed to the synergistic effect of nanoencapsulations along with the utilization of hollow MNs that ensured effective TER transdermal delivery to the affected joints.

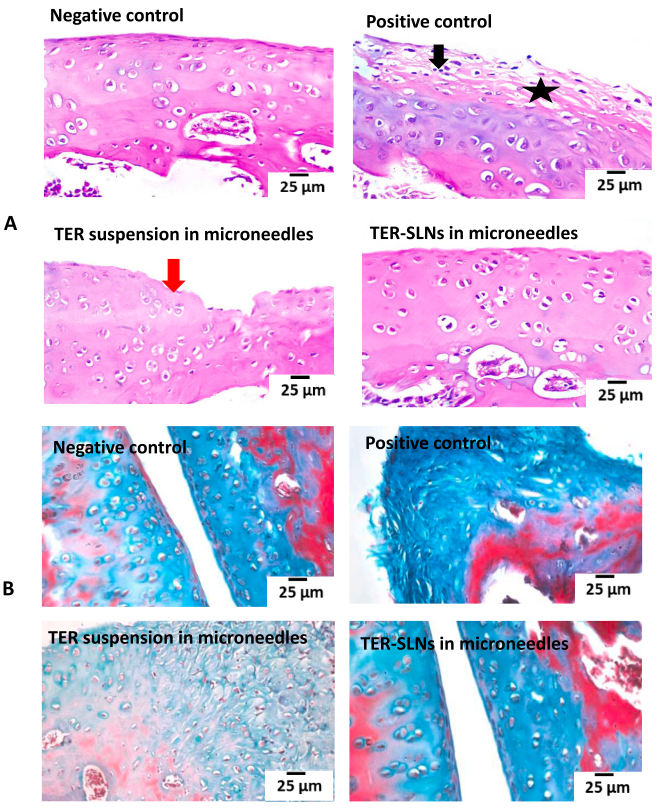

Fig. 7. Histological examination of dissected joints after staining with (A) Hematoxylin and eosin and (B) Masson Trichrome stain. Black arrow illustrates infiltration of mononuclear inflammatory cells, star illustrates fibrous connective tissue and red arrow illustrates severe destruction of articular surface. The scale marker corresponds to 25 µm. (For interpretation of the references to colour in this figure legend, the reader is referred to the web version of this article.)

5. Conclusion

This work opens new avenues for the applications of SLNs and hollow MNs. TER-SLNs were successfully prepared using the melt emulsification technique with monomodal particle size distribution, uniform spherical shape and high EE%. The prepared SLNs achieved sustained TER release over 96 h. In arthritic rats, the group treated w TER-SLNs using AdminPen™ hollow MNs showed comparable levels of inflammatory biomarkers to negative control. Collectively, the obtained results of joint morphology, diameter measurements, ELISA and histopathological examination revealed the superiority of the TER-SLNs and AdminPen™ hollow MNs combined system in reducing inflammation and healing RA in rats. In future, this innovative combination system could represent a promising painless and self-administrating alternative modality for the currently used invasive intra-articular injections. Potentially, MNs and nanotechnology platforms could be considered as the next generation of anti-arthritic drug delivery systems.

Declaration of Competing Interest

The authors declare that they have no known competing financial interests or personal relationships that could have appeared to influence the work reported in this paper.

Data availability

The authors do not have permission to share data.

References

Abbas, H., Refai, H., El Sayed, N., 2018. Superparamagnetic iron oxide–loaded lipid nanocarriers incorporated in thermosensitive in situ gel for magnetic brain targeting of clonazepam. J. Pharm. Sci. 107 (8), 2119–2127.

Abbas, H., El-Deeb, N.M., Zewail, M., 2021. PLA-coated Imwitor® 900 K-based herbal colloidal carriers as novel candidates for the intra-articular treatment of arthritis. Pharm. Dev. Technol. 26 (6), 682–692.

Abbas, H., Refai, H., El Sayed, N., Rashed, L.A., Mousa, M.R., Zewail, M., 2021. Superparamagnetic iron oxide loaded chitosan coated bilosomes for magnetic nose to brain targeting of resveratrol. Int. J. Pharm. 610, 121244.

Abbas, H., Gad, H.A., El Sayed, N.S., Rashed, L.A., Khattab, M.A., Noor, A.O., Zewail, M., 2022. Development and evaluation of novel leflunomide SPION bioemulsomes for the intra-articular treatment of arthritis. Pharmaceutics 14 (10), 2005.

Abd, E., et al., 2016. Skin models for the testing of transdermal drugs. Clinical pharmacology: advances and applications 8, 163.

Abd-El-Azim, H., Tekko, I.A., Ali, A., Ramadan, A., Nafee, N., Khalafallah, N., Rahman, T., Mcdaid, W., Aly, R.G., Vora, L.K., Bell, S.J., Furlong, F., McCarthy, H.O., Donnelly, R.F., 2022. Hollow microneedle assisted intradermal delivery of hypericin lipid nanocapsules with light enabled photodynamic therapy against skin cancer. J. Control. Release 348, 849–869.

Ahmed, S., Kassem, M.A., Sayed, S., 2020. Bilosomes as promising nanovesicular carriers for improved transdermal delivery: construction, in vitro optimization, ex vivo permeation and in vivo evaluation. Int. J. Nanomed. 15, 9783.

Alimardani, V., Abolmaali, S.S., Yousefi, G., Rahiminezhad, Z., Abedi, M., Tamaddon, A., Ahadian, S., 2021. Microneedle arrays combined with nanomedicine approaches for transdermal delivery of therapeutics. J. Clin. Med. 10 (2), 181.

Anita, C., et al., 2021. Topical nanocarriers for management of rheumatoid arthritis: a review. Biomed. Pharmacother. 141, 111880.

Boskabady, M.H., et al., 2011. Pharmacological effects of Rosa damascena. Iran. J. Basic Med. Sci. 14 (4), 295.

Bushra, F., 2020. Delivery of Denosumab via Hollow Microneedle. 2020, Brac University.

Carcamo-Martinez, A., et al., 2021. Enhancing intradermal delivery of tofacitinib citrate: Comparison between powder-loaded hollow microneedle arrays and dissolving microneedle arrays. Int. J. Pharm. 593, 120152.

Chadha, S., Behl, T., Kumar, A., Khullar, G., Arora, S., 2020. Role of Nrf2 in rheumatoid arthritis. Current Research in Translational Medicine 68 (4), 171–181.

Chaturvedi, V., et al., 1999. Estimation & significance of serum & synovial fluid malondialdehyde levels in rheumatoid arthritis. Indian J. Med. Res. 109, 170.

Choudhary, N., Bhatt, L.K., Prabhavalkar, K.S., 2018. Experimental animal models for rheumatoid arthritis. Immunopharmacol. Immunotoxicol. 40 (3), 193–200.

Churchman, S., Ponchel, F., 2008. Interleukin-7 in rheumatoid arthritis. Rheumatology 47 (6), 753–759.

Dragicevic-Curic, N., Gräfe, S., Gitter, B., Winter, S., Fahr, A., 2010. Surface charged temoporfin-loaded flexible vesicles: in vitro skin penetration studies and stability. Int. J. Pharm. 384 (1-2), 100–108.

El-Nabarawi, M.A., Shamma, R.N., Farouk, F., Nasralla, S.M., 2020. Bilosomes as a novel carrier for the cutaneous delivery for dapsone as a potential treatment of acne: preparation, characterization and in vivo skin deposition assay. J. Liposome Res. 30 (1), 1–11.

El-Sayyad, N.-M., Badawi, A., Abdullah, M.E., Abdelmalak, N.S., 2017. Dissolution enhancement of leflunomide incorporating self emulsifying drug delivery systems and liquisolid concepts. Bulletin of Faculty of Pharmacy, Cairo University 55 (1), 53–62.

El-Setouhy, D.A., Abdelmalak, N.S., Anis, S.E., Louis, D., 2015. Leflunomide biodegradable microspheres intended for intra-articular administration: Development, anti-inflammatory activity and histopathological studies. Int. J. Pharm. 495 (2), 664–670.

Fadda, S., Abolkheir, E., Afifi, R., Gamal, M., 2016. Serum matrix metalloproteinase-3 in rheumatoid arthritis patients: Correlation with disease activity and joint destruction. The Egyptian Rheumatologist 38 (3), 153–159.

Fernandes, R.M.S.N., Da Silva, N.P., Sato, E.I., 2012. Increased myeloperoxidase plasma levels in rheumatoid arthritis. Rheumatol. Int. 32 (6), 1605–1609.

Ferrándiz, M.L., Nacher-Juan, J., Alcaraz, M.J., 2018. Nrf2 as a therapeutic target for rheumatic diseases. Biochem. Pharmacol. 152, 338–346.

Ghasemiyeh, P., Mohammadi-Samani, S., 2018. Solid lipid nanoparticles and nanostructured lipid carriers as novel drug delivery systems: Applications, advantages and disadvantages. Research in pharmaceutical sciences 13 (4), 288.

Gorantla, S., Batra, U., Puppala, S.RN.E.R., Waghule, T., Naidu, V.G.M., Singhvi, G., 2022. Emerging trends in microneedle-based drug delivery strategies for the treatment of rheumatoid arthritis. Expert Opin. Drug Deliv. 19 (4), 395–407.

Gottenberg, J.-E., et al., 2019. Comparative effectiveness of rituximab, abatacept, and tocilizumab in adults with rheumatoid arthritis and inadequate response to TNF inhibitors: prospective cohort study. Bmj, **364**.

Grönwall, C., Amara, K., Hardt, U., Krishnamurthy, A., Steen, J., Engström, M., Sun, M., Ytterberg, A.J., Zubarev, R.A., Scheel-Toellner, D., Greenberg, J.D., Klareskog, L., Catrina, A.I., Malmström, V., Silverman, G.J., 2017. Autoreactivity to malondialdehyde-modifications in rheumatoid arthritis is linked to disease activity and synovial pathogenesis. J. Autoimmun. 84, 29–45.

I Keen, H., Conaghan, P.G., Tett, S.E., 2013. Safety evaluation of leflunomide in rheumatoid arthritis. Expert Opin Drug Saf. 12 (4), 581–588.

Kamel, R., Salama, A.H., Mahmoud, A.A., 2016. Development and optimization of self-assembling nanosystem for intra-articular delivery of indomethacin. Int. J. Pharm. 515 (1–2), 657–668.

Kirsch, B.M., et al., 2005. The active metabolite of leflunomide, A77 1726, interferes with dendritic cell function. ArthritisResearchTher. 7 (3), 1–10.

Kobayashi, Y., Ueyama, S., Arai, Y., Yoshida, Y., Kaneda, T., Sato, T., Shin, K., Kumegawa, M., Hakeda, Y., 2004. The active metabolite of leflunomide, A771726, inhibits both the generation of and the bone-resorbing activity of osteoclasts by acting directly on cells of the osteoclast lineage. Journal of Bone and MineralMetab. 22 (4).

Kutukculer, N., Caglayan, S., Aydogdu, F., 1998. Study of pro-inflammatory (TNF-α, IL-1α, IL-6) and T-cell-derived (IL-2, IL-4) cytokines in plasma and synovial fluid of patients with juvenile chronic arthritis: correlations with clinical and laboratory parameters. Clin. Rheumatol. 17 (4), 288–292.

Larraneta, E., et al., 2016. Microneedle arrays as transdermal and intradermal drug delivery systems: Materials science, manufacture and commercial development. Mater. Sci. Eng. R. Rep. 104, 1–32.

Larrañeta, E., Moore, J., Vicente-Pérez, E.M., González-Vázquez, P., Lutton, R., Woolfson, A.D., Donnelly, R.F., 2014. A proposed model membrane and test method for microneedle insertion studies. Int. J. Pharm. 472 (1-2), 65–73.

Lastow, O., Iconovo, A., Village, M., 2015. Future Patient Requirements on Inhalation Devices: The Balance between Patient, Commercial, Regulatory and Technical Requirements. Advances and Challenges, Pulmonary Drug Delivery, pp. 339–352.

Liu, Y.-L., et al., 2009. Suppression of complete Freund's adjuvant-induced adjuvant arthritis by cobratoxin. Acta. Pharmacol. Sin. 30 (2), 219–227.

Mistry, K., Sarker, D., 2016. SLNs can serve as the New Brachytherapy Seed: Determining Influence of Surfactants on Particle Size of Solid Lipid Microparticles and Development of Hydrophobised Copper Nanoparticles for Potential Insertion. J Chem Eng Process Technol 7, 302.

Ng, W.K., Saiful Yazan, L., Yap, L.H., Wan Nor Hafiza, W.A.G., How, C.W., Abdullah, R., 2015. Thymoquinone-loaded nanostructured lipid carrier exhibited cytotoxicity towards breast cancer cell lines (MDA-MB-231 and MCF-7) and cervical cancer cell lines (HeLa and SiHa). BioMed Research International 2015, 1–10.

Odobasic, D., Yang, Y., Muljadi, R.C.M., O'Sullivan, K.M., Kao, W., Smith, M., Morand, E. F., Holdsworth, S.R., 2014. Endogenous Myeloperoxidase Is a Mediator of Joint Inflammation and Damage in Experimental Arthritis. Arthritis & Rheumatology 66 (4), 907–917.

Onugwu, A.L., et al., 2022. Development and optimization of solid lipid nanoparticles coated with chitosan and poly (2-ethyl-2-oxazoline) for ocular drug delivery of ciprofloxacin. J. Drug Delivery Sci. Technol. 74, 103527.

Osiri, M., et al., 2003. Leflunomide for the treatment of rheumatoid arthritis: a systematic review and metaanalysis. J. Rheumatol. 30 (6), 1182–1190.

Rahman, H.S., et al., 2013. Zerumbone-loaded nanostructured lipid carriers: preparation, characterization, and antileukemic effect. Int. J. Nanomed. 8, 2769.

Ross, R.F., *Device for delivery of rheumatoid arthritis medication.* 2016, Google Patents.

Saedi, A., Rostamizadeh, K., Parsa, M., Dalali, N., Ahmadi, N., 2018. Preparation and characterization of nanostructured lipid carriers as drug delivery system: Influence of liquid lipid types on loading and cytotoxicity. Chem. Phys. Lipids 216, 65–72.

Sanders, S., Harisdangkul, V., 2002. Leflunomide for the treatment of rheumatoid arthritis and autoimmunity. Am J M Sc. 323 (4), 190–193.

Shang, H., Younas, A., Zhang, N., 2022. Recent advances on transdermal delivery systems for the treatment of arthritic injuries: From classical treatment to nanomedicines. Wiley Interdisciplinary Reviews: Nanomedicine and Nanobiotechnology 14 (3), e1778.

Sun, S., Bay-Jensen, A.-C., Karsdal, M.A., Siebuhr, A.S., Zheng, Q., Maksymowych, W.P., Christiansen, T.G., Henriksen, K., 2014. The active form of MMP-3 is a marker of synovial inflammation and cartilage turnover in inflammatory joint diseases. BMC Musculoskelet. Disord. 15 (1).

Üner, M., Yener, G., 2007. Importance of solid lipid nanoparticles (SLN) in various administration routes and future perspectives. Int. J. Nanomed. 2 (3), 289.

Venkatesh, T., et al., 2011. Nanosuspensions: ideal approach for the drug delivery of poorly water soluble drugs. Der. Pharm. Lett. 3 (2), 203–213.

Vyas, S., Sharma, H., V. rk,, 2016. *ROLE OF MALONDIALDEHYDE IN THE SERUM OF RHEUMATOID ARTHRITIS AND OSTEOARTHRITIS.* JPMI. Journal of Postgraduate Medical Institute 30 (1).

Wang, Q., Qin, X., Fang, J., Sun, X., 2021. Nanomedicines for the treatment of rheumatoid arthritis: State of art and potential therapeutic strategies. Acta Pharmaceutica Sinica B 11 (5), 1158–1174.

Wang, J., Zeng, J., Liu, Z., Zhou, Q., Wang, X., Zhao, F., Zhang, Y.u., Wang, J., Liu, M., Du, R., 2022. Promising Strategies for Transdermal Delivery of Arthritis Drugs: Microneedle Systems. Pharmaceutics 14 (8), 1736.

Yang, J., Liu, X., Fu, Y., Song, Y., 2019. Recent advances of microneedles for biomedical applications: drug delivery and beyond. Acta Pharmaceutica Sinica B 9 (3), 469–483.

Yuzhakov, V.V., 2010. The AdminPen™ microneedle device for painless & convenient drug delivery. Drug Delivery Technology 10 (4), 32–36.

Yuzhakov, V.V., *Microneedle array, patch, and applicator for transdermal drug delivery.* 2010, https://patents.google.com/patent/WO2007081430A3/en.

Zewail, M., et al., 2019. Coated nanostructured lipid carriers targeting the joints–an effective and safe approach for the oral management of rheumatoid arthritis. Int. J. Pharm. 567, 118447.
Zewail, M., 2021. Folic acid decorated chitosan-coated solid lipid nanoparticles for the oral treatment of rheumatoid arthritis. Ther. Deliv. 12 (4), 297–310.
Zewail, M., et al., 2022. Hyaluronic acid coated teriflunomide (A771726) loaded lipid carriers for the oral management of rheumatoid arthritis. Int. J. Pharm. 623, 121939.
Zewail, M., Nafee, N., Boraie, N., 2021. Intra-articular dual drug delivery for synergistic rheumatoid arthritis treatment. J. Pharm. Sci. 110 (7), 2808–2822.
Zewail, M., E. Gaafar, P.M., Ali, M.M., Abbas, H., 2022. Lipidic cubic-phase leflunomide nanoparticles (cubosomes) as a potential tool for breast cancer management. Drug Deliv. 29 (1), 1663–1674.
Zhang, W., Zhang, W., Li, C., Zhang, J., Qin, L., Lai, Y., 2022. Recent advances of microneedles and their application in disease treatment. Int. J. Mol. Sci. 23 (5), 2401.
Zheng, M., Jia, H., Wang, H., Liu, L., He, Z., Zhang, Z., Yang, W., Gao, L., Gao, X., Gao, F., 2021. Application of nanomaterials in the treatment of rheumatoid arthritis. RSC Adv. 11 (13), 7129–7137.
Zirak, M.B., Pezeshki, A., 2015. Effect of surfactant concentration on the particle size, stability and potential zeta of beta carotene nano lipid carrier. International JournalCurr. Microbiol. App. Sci. 4 (9), 924–932.